Supplementary material

Switching spin and charge between edge states in topological insulator constrictions

Viktor Krueckl and Klaus Richter

Institut für Theoretische Physik, Universität Regensburg, D-93040 Regensburg, Germany

July 1, 2011

In Reference [1] we show how to employ HgTe-based constrictions in order to steer the charge flow and to switch between different spin orientations of the edges states in bulk two-dimensional HgTe. Here we give more details on the model and the HgTe material parameters used, as well as on our numerical transport calculations.

A Confined Eigenstates

The one-dimensional effective Hamiltonian in our manuscript [1] is based on the four different edge states of the Hamiltonian [2]

$$H = \begin{pmatrix} M-(B+D)\boldsymbol{k}^2 & Ak_+ & & \\ Ak_- & -M+(B-D)\boldsymbol{k}^2 & & \\ & & M-(B+D)\boldsymbol{k}^2 & -Ak_- \\ & & -Ak_+ & -M+(B-D)\boldsymbol{k}^2 \end{pmatrix} \tag{8}$$

where the motion is confined to a quasi one-dimensional system of a constant width W (with $k_\pm = k_x \pm \mathrm{i}k_y$ and $\boldsymbol{k}^2 = k_x^2 + k_y^2$). To model HgTe we use the material parameters[3, 4] summarized in Table 1. We have chosen the lead to point along the x-direction and search for the transversal eigenfunctions $\psi(y)$. In order to obtain those states we impose boundary conditions separately for the lower and upper side,

$$\psi(y \leq 0) = 0 \quad ; \quad \psi(y \geq W) = 0\,, \tag{9}$$

respectively, and use exponential decaying trial functions $\psi_\uparrow = \mathrm{e}^{-\lambda y}(1 \quad -\xi \quad 0 \quad 0)$ and $\psi_\downarrow = \mathrm{e}^{-\lambda y}(0 \quad 0 \quad 1 \quad \xi)$ with a momentum k_y in lead direction. This leads to two decay lengths

$$\lambda_1^\pm = \sqrt{k_x^2 + F^\pm + \sqrt{\frac{M^2-(E^\pm)^2}{B^2-D^2}}}, \tag{10}$$

$$\lambda_2^\pm = \sqrt{k_x^2 + F^\pm - \sqrt{\frac{M^2-(E^\pm)^2}{B^2-D^2}}}, \tag{11}$$

with

$$F^\pm = \frac{A^2 - 2(MB + E^\pm D)}{2(B^2 - D^2)}. \tag{12}$$

Since $\lambda_2^\pm \gg \lambda_1^\pm$ inside the gap the parts of the wavefunction with $\lambda_2^\pm$ can be neglected in the following. The superscript indicates the propagation direction of the states where $(+)$ stands for a right-moving state and $(-)$ for a left-moving one. This direction depends on the group velocity given by the corresponding energy dispersion

$$E^\pm = \frac{\mp A\sqrt{B^2 - D^2}k_x - DM}{B}. \tag{13}$$

Additionally, we find the weight of the second spinor entry to be

$$\xi^\pm = \mp\frac{A^2 + 2BE^\pm + 2DM + G^\pm}{4A(E^\pm) + M}\left(-2H^\pm + \sqrt{2\frac{A^2-G-2B(M-B(H^\pm)^2-2D(E^\pm-D(D^\pm)^2))}{(B-D)(B+D)}}\right) \tag{14}$$

with the energy dependent functions

$$G^\pm = \sqrt{A^4 - 4A^2(DE^\pm + BM) + 4(BE^\pm + DM)^2}, \tag{15}$$

$$H^\pm = \frac{BE^\pm + DM}{A\sqrt{B^2 - D^2}}. \tag{16}$$

A	B	D	M	Δ	$R/(e\mathcal{E}_z)$
354.5	-686	-512	-10	1.6	-15.6

Table 1: Material parameters for HgTe (units in meV and nm)[3, 4].

The resulting four eigenstates are given by

$$\psi_{\uparrow}^{+}(y) \propto \left(\mathrm{e}^{\lambda_1^+(y-W)} - \mathrm{e}^{\lambda_2^+(y-W)}\right) \quad \begin{pmatrix} 1 & -\xi^+ & 0 & 0 \end{pmatrix}, \tag{17a}$$

$$\psi_{\uparrow}^{-}(y) \propto \left(\mathrm{e}^{-\lambda_1^-y} - \mathrm{e}^{-\lambda_2^-y)}\right) \quad \begin{pmatrix} 1 & -\xi^- & 0 & 0 \end{pmatrix}, \tag{17b}$$

$$\psi_{\downarrow}^{+}(y) \propto \left(\mathrm{e}^{-\lambda_1^+y} - \mathrm{e}^{-\lambda_2^+y}\right) \quad \begin{pmatrix} 0 & 0 & 1 & \xi^+ \end{pmatrix}, \tag{17c}$$

$$\psi_{\downarrow}^{-}(y) \propto \left(\mathrm{e}^{\lambda_1^-(y-W)} - \mathrm{e}^{\lambda_2^-(y-W)}\right) \quad \begin{pmatrix} 0 & 0 & 1 & \xi^- \end{pmatrix}, \tag{17d}$$

and are used as the basis of the effective one-dimensional Hamiltonian (6) in the manuscript. Furthermore these states are employed to derive the confinement induced mass gap[5] and the strength of the spin-orbit interaction. The spin-orbit interaction due to bulk-inversion asymmetry (BIA) enters the full Hamiltonian as

$$H_{\mathrm{BIA}} = \begin{pmatrix} & & & -\Delta \\ & & \Delta & \\ & \Delta & & \\ -\Delta & & & \end{pmatrix} \tag{18}$$

with the momentum independent splitting Δ. The matrix element for spin-orbit interaction in the effective Hamiltonian is given by

$$\delta^{\pm} = \langle \psi_{\uparrow}^{\pm} | H_{\mathrm{BIA}} | \psi_{\downarrow}^{\pm} \rangle \approx -\frac{4\mathrm{e}^{-\lambda^{\pm}W}\lambda^{\pm}W\xi^{\pm}}{1+(\xi^{\pm})^2}\Delta. \tag{19}$$

If the width of the quasi one-dimensional lead is small, the spin-orbit interaction grows since a non-vanishing overlap between the two right-moving and the two left-moving states of different subblocks appears. For a wide enough lead ($W \gtrsim 1000$nm) the spin-orbit interaction vanishes exponentially, thus the states can be chosen spin-polarized within this limit.

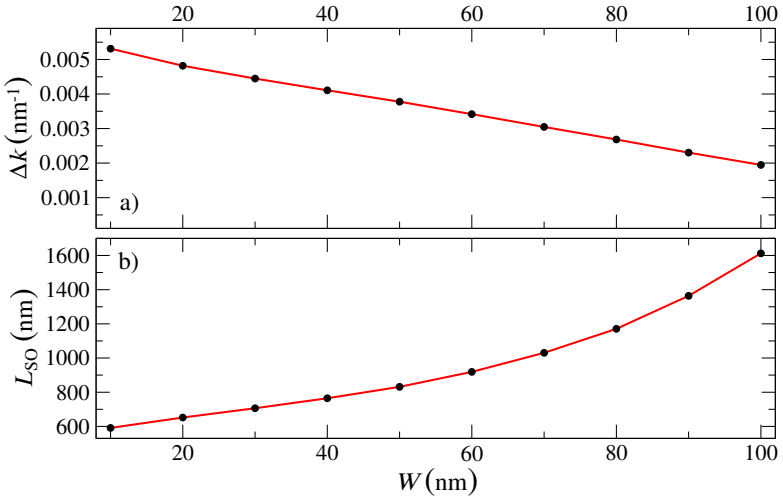

Figure 4: Spin precession length for different constriction widths – a) Momentum difference between the spin-split topological states closed to the confinement induced gap, extracted from bandstructure calculations. b) Resulting spin precession length L_{SO} for different constriction widths.

B Relation between constriction width and spin-precession length

The spin-transistor effect is present for a conducting constriction at energies below

$$E_0 = -\frac{MD}{B} - m(W)$$

where the parameters M, D, B are defined in Eq. (1) and the confinement induced gap $m(W)$ is given approximately by Eq. (4). Using the effective spin-orbit interaction $\delta^{\pm}$, Eq. (5), for this energy E_0, one can estimate the spin precession length $L_{\mathrm{SO}} \approx \pi a/\delta^{\pm}$ and the corresponding channel length. For usual HgTe material parameters, the shortest channel length of about 700 nm can be achieved for constriction widths of $40-50$ nm. However this estimate, based on the approximations Eq. (4, 5) is only valid for wide enough constrictions.

Therefore we performed band-structure calculations for the infinitely extended constriction of different widths W and extracted the band-splitting Δk (Fig. 4(a)) at the top of the hole-like edge-state bands, which results in the spin precession length $L_{\mathrm{SO}} = \pi/\Delta k$ shown in Fig. 4(b). These full two-dimensional calculations show a decreasing spin-precession length L_{SO} reaching $L_{\mathrm{SO}} = 600$ nm at channel widths of 10 nm. For narrower channels, the confinement induced mass gap increases and sets another limit for the optimal channel width.

At a width of 30 nm the confinement induced gap already spans half of the bulk bandgap. Thus scaling down to lower withs also affects the operating range of the spin-transistor.

Another parameter to tune the necessary constriction length, besides the its width, is the strength of the SOI itself. Thus tuning the material and the heterostructure producing the two-dimensional confinement is a second option to increase the spin-orbit interaction and reduce the necessary channel lengths in return.

C Wave-packet transport algorithm

The transport properties through the HgTe constrictions presented in this manuscript are calculated by a wave-packet algorithm. Roughly speaking, such a scheme exploits the fact that a spatially localized wave-packet contains a broad energy range. Thus an exact time-evolution of such an initial state depends on the full energy dependent scattering matrix for the stationary scattering problem considered. Consequently the goal of the following section is the extraction of the scattering matrix from the time-evolution of a wave-packet. The scheme has the advantage of calculating the full energy dependent scattering matrix from a single wave-packet propagation, provided that the initial wave-packet is chosen properly.

We start by numerically calculating the transversal wavefunktions $\chi_n(x,k)$ within the asymptotic lead regions for different longitudinal wave-vectors k. From the resulting dispersion $E_n(k)$ we derive the group velocity $v_n = \partial E_n(k)/\hbar\partial k$ and select incoming and outgoing states. Additionally, the transversal wavefunctions are grouped into modes with a group index ν by maximizing their overlap $\langle\chi_\nu(x,k)|\chi_n(x,k+\delta k)\rangle$ for small δk and all n. Degenerate states are classified by their spin-polarization. In the case of HgTe we use a subblock spin-polarization matrix $\mathcal{S} = \sigma_z \otimes \mathbb{I}$. This allows for the calculation of incoming $(+)$ and outgoing $(-)$ wave-packets for different modes ν by the Fourier transformation

$$\Phi_\nu^\pm(x,y) = \int_{-\infty}^{\infty} \eta_\nu(k)\ \chi_\nu^\pm(x,k)\ \mathrm{e}^{\mathrm{i}ky}\ \mathrm{d}k \tag{20}$$

where $\eta_\nu(k)$ is a weighting function to restrict the energy distribution to a certain window. The exact functional form of $\eta_\nu(k)$ is somewhat arbitrary, but should be chosen in a way to ensure a localized wave-packet, like a Gaussian distribution or a sum of two Fermi functions. The resulting incoming wave-packet is then placed into the asymptotic region of the system, as shown in Fig. 5(a). In order to get a row of the scattering matrix $S_{\beta,\alpha}(E)$ we take all

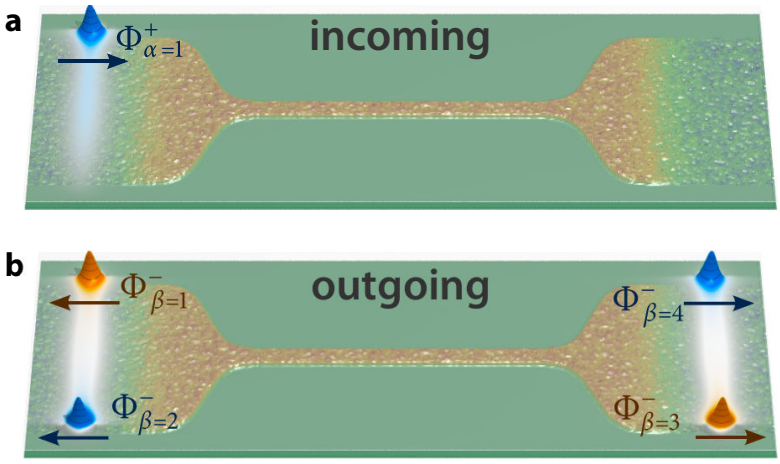

Figure 5: Wave-packet setup for a transport calculation – a) Initial incoming wave-packet in the asymptotic region of a HgTe constriction whose time-evolution needs to be calculated. b) Different outgoing wave-packets in the asymptotic region of a HgTe constriction needed for the overlap with the propagating incoming wave-packet.

outgoing wave-packets $\Phi(x,y)^-_\beta$, as shown in Fig. 5(b), and calculate the overlap

$$C_{\beta,\alpha}(t) = \langle \Phi(x,y)^-_\beta | \hat{U}(t) | \Phi(x,y)^+_\alpha \rangle \tag{21}$$

with the time-evolution of an incoming wave-packet $\Phi(x,y)^+_\alpha$. In our numerical implementation the time-evolution operator $\hat{U}(t) = \exp\left(-\mathrm{i}\hat{H}t/\hbar\right)$ is expressed by an expansion in terms of Chebyshev polynomials $\mathrm{Ch}_n(\hat{H})$ of the Hamilton operator. Thus the time-evolution is given by the sum

$$\hat{U}(t)|\Phi(x,y)^+_\alpha\rangle = \sum_{n=0}^{N} a_n \left(\frac{\Delta E t}{2\hbar}\right) \underbrace{\mathrm{Ch}_n(-\mathrm{i}\hat{H}_{\mathrm{norm}})|\Phi(x,y)^+_\alpha\rangle}_{P_n} \tag{22}$$

with a normalized Hamiltonian $\hat{H}_{\mathrm{norm}} = 2\hat{H}/\Delta E$ to map the energy spectrum of the system into the interval $[-1,1]$. The polynomials P_n are given by the recursion relations

$$P_0 = |\Phi(x,y)^+_\alpha\rangle, \tag{23a}$$
$$P_1 = \hat{H}_{\mathrm{norm}}|\Phi(x,y)^+_\alpha\rangle, \tag{23b}$$
$$P_n = -2\mathrm{i}\hat{H}_{\mathrm{norm}}P_{n-1} + P_{n-2} \tag{23c}$$

and the expansion coefficients by Bessel functions

$$a_n(\alpha) = \frac{2-\delta_{n,0}}{\pi}\int_{-1}^{1}\frac{\exp(-\mathrm{i}\alpha x)\mathrm{Ch}_n(x)}{\sqrt{1-x^2}}\mathrm{d}x = (2-\delta_{n,0})(-i)^n J_n(\alpha). \tag{24}$$

Since only powers of the Hamiltonian are needed and no matrix inversions, like in a recursive Green function algorithm, we can use a mixed representation in position and momentum space[6]. The mixed representation avoids a discretized derivative operator and thus the fermion doubling problem. As a result we can even propagate the wave-packets on a bare Dirac equation[7]. Additionally avoiding matrix inversions leads to a favorable computational scaling.

After the initial wave-packet has left the scattering region, we use the time-dependent correlation $C_{\beta,\alpha}(t)$ to get the scattering matrix

$$S_{\beta,\alpha}(E) = \frac{\sqrt{v_\alpha(E)v_\beta(E)}}{(2\pi\hbar)^2\ \eta_\alpha(E)\eta_\beta(E)}\int_{-\infty}^{\infty} C_{\beta,\alpha}(t)e^{\mathrm{i}Et/\hbar}\mathrm{d}t \tag{25}$$

by means of a second Fourier transformation. A direct comparison with another, independent transport algorithm using Green functions[8] shows a very good agreement between both approaches. Since the whole energy dependence of the scattering matrix is needed in our considerations we benefit from the wave-packet algorithm.

Furthermore the wave-packet scheme is not restricted to scattering amplitudes, but can also be used to calculate observables within the system, like for example the non-equilibrium local density for a state entering at a certain lead, as shown in Fig. 1(a-c) of the manuscript[1]. In order to get the state ψ_E at the Fermi energy E one has to integrate the propagating wave-packet $\hat{U}(t)\ \Phi^+_\alpha(x,y)$ during the time-evolution,

$$\psi_E(x,y) = \int \hat{U}(t)\ \Phi^+_\alpha(x,y)\ e^{\mathrm{i}Et/\hbar}\mathrm{d}t. \tag{26}$$

This can be done for several different energies during one wavepacket run, leading at once to all the different switching states shown in Fig. 1(a-c) of Ref. [1].

Impurities and wall roughness

In order to take impurities into account, we add a electrostatic impurity potential

$$U_{\mathrm{imp}}(\boldsymbol{r}) = \sum_n U_n \mathrm{e}^{-\frac{|r-r_n|^2}{2\rho^2}} \tag{27}$$

given by a random potential U_n chosen Gaussian distributed on every single grid-point and Gaussian correlated on the length scale $\rho = 10$ nm. The strength of the potential is determined by $\langle U_{\mathrm{imp}}(\boldsymbol{r})^2\rangle = U_0^2$. The roughness of the walls, which is unavoidable in experiments due to the necessary etching processes, is modeled by a randomly changing edge position. To this end we define the width of the strip separately for the right and the left side by

$$W_{\mathrm{rand}}(x) = W(x) + \sum_i W_i \sin(x/l_i + \theta_i) \tag{28}$$

where $W(x)$ is the smooth variation of the constriction given by Eq. (7) of the manuscript. For the presented calculations we use l_i varying from 10 nm to 30 nm with a step size of 1 nm and uniformly distributed random phases θ_i. The amplitudes W_i are chosen uniformly to create a maximal deviation

$$W_r = \max(|W_{\mathrm{rand}}(x) - W(x)|) \tag{29}$$

of 20 nm for top-gate switching presented in Fig. 3(a-d) as well as 10 nm for the side-gate switching in Fig. 3(e-h). The deviation W_r is hence considerable on the scales of the constriction widths of 100 and 60 nm respectively.

References

[1] V. Krueckl and K. Richter, *Switching spin and charge between edge states in topological insulator constrictions*, ??? **??**, ?? (2011).

[2] B. A. Bernevig, T. L. Hughes and S.-C. Zhang, *Quantum Spin Hall Effect and Topological Phase Transition in HgTe Quantum Wells*, Science **314**, 1757 (2006).

[3] M. König *et al.*, *The Quantum Spin Hall Effect: Theory and Experiment*, J. Phys. Soc. Jpn. **77**, 031007 (2008).

[4] D. G. Rothe *et al.*, *Fingerprint of different spin–orbit terms for spin transport in HgTe quantum wells*, New J. Phys. **12**, 065012 (2010).

[5] B. Zhou *et al.*, *Finite Size Effects on Helical Edge States in a Quantum Spin-Hall System*, Phys. Rev. Lett. **101**, 246807 (2008).

[6] M. Feit, J. F. Jr. and A. Steiger, *Solution of the Schroedinger equation by a spectral method*, J. Comp. Phys. **47**, 412 (1982).

[7] V. Krueckl and T. Kramer, *Revivals of quantum wave packets in graphene*, New J. Phys. **11**, 093010 (2009).

[8] M. Wimmer and K. Richter, *Optimal block-tridiagonalization of matrices for coherent charge transport*, J. Comput. Phys. **228**, 8548 (2009).